**Paweł Baranowski,
Jerzy Małachowski,
Tadeusz Niezgoda,
Łukasz Mazurkewicz**

Dynamic behaviour of Various Fibre Systems During Impact Interaction – Numerical Approach

DOI: 10.5604/12303666.1167423

**Military University of Technology,
Faculty of Mechanical Engineering,
Department of Mechanics
and Applied Computer Science,**
ul. S. Kaliskiego 2, 00-908 Warsaw, Poland
E-mail: pawel.baranowski@wat.edu.pl

Abstract
The paper presented shows a part of investigations covering the contact problem in numerical modelling using an explicit code. The authors have outlined the parameters and factors that have a direct impact on a proper contact definition, which, as is known, has much importance in finite element analyses. For the purpose of the study, a test model was proposed, where an interaction between a net and chosen 3D object with relatively small geometric dimensions and low weight was simulated. Additionally several net structures were analysed in which their contact characteristic was modified. Different interaction conditions in each case resulted in a different influence on the 3D object's behaviour, especially its velocity and trajectory changes.

Key words: *contact procedure, dynamics, explicit analyses.*

Symbols used

$\overline{\mathbf{a}}_\alpha\left(\overline{\xi}^1,\overline{\xi}^2\right)$ - *tangent covariant base vectors (α = 1,2)*
$\overline{a}_{\alpha\beta}=\overline{\mathbf{a}}_\beta\cdot\overline{\mathbf{a}}_\alpha$ - *metric tensor*
A_k - *area of contact element*
$\boldsymbol{b}$ - *left Cauchy-Green deformation tensor*
$B^{(1)}$, $B^{(2)}$ - *bodies in contact*
C - *scale factor related to CFL condition*
C_c - *contact contribution*
D_c - *exponential coefficient*
$\mathbf{F}_c$ - *contact force vector*
$F_{f1}, ..., F_{fi}$ - *frictional force*
$\boldsymbol{F}_N$ - *normal force*
$F_{T1}, ..., F_{Ti}$ - *tangential force*
g_N - *normal gap (penetration)*
g_T - *tangential relative displacement*
$\mathbf{K}_c$ - *contact stiffness matrix*
$k_{cs}(t)$ - *stability contact stiffness*
k_{fibre} - *resultant stiffness of net fibre*
$\mathbf{K}_N$ - *normal contact matrix*
k_{object} - *resultant stiffness of the solid of revolution*
$k'_{s1}, ..., k'_{si}$ - *stiffness of fictional elastic element*
$k_{soft=1}$ - *contact stiffness in soft contact procedure*
$\mathbf{K}_T^{slip}$ - *tangent stiffness matrix for slip case*
$\mathbf{K}_T^{stick}$ - *symmetric tangent stiffness matrix*
m - *function dependent on masses of master and slave nodes*
$\overline{\mathbf{n}}$ - *normal to master face* $\Gamma_c^{(2)}$
$\ddot{q}_t, \dot{q}_t, q_t$ - *acceleration, velocity, displacement at t time respectively*
$r(t)$ - *displacement of 3D body*
S_{soft} - *scaling factor*
t - *time*
$\overline{\mathbf{t}}$ - *contact stress tensor*
$\overline{t}_N$ - *normal stress*
$\overline{t}_T$ - *tangential stress*
$t_{T\alpha}^{stick}$ - *tangential stress in stick phase*
$t_{T\alpha}^{slip}$ - *tangential stress in slip phase*
v_{body} - *transitional velocity of 3D body*
v_{net} - *transitional velocity of net*
V_W - *relative velocity between bodies*
$\overline{\mathbf{x}}$ - *projection point of current position*
x^k - *slave node*
$\delta\mathbf{u}_c^T$ - *displacement vector*
Δt_{cs} - *initial solution time step*
Δt_{con} - *time step size depending on the contact procedure*
Δt_{FE} - *time step determined by minimum value over elements*
ε_N - *normal penalty factor*
ε_T - *tangential penalty factor*
$\Gamma_c^{(i)}$, $\Gamma_c^{(2)}$ - *contact surfaces*
μ - *friction coefficient*
μ_D - *dynamic friction coefficient*
μ_S - *static friction coefficient*
σ - *stress tensor*
ω_{body} - *rotational velocity of 3D body*
ω_{net} - *rotational velocity of net*

Introduction

The paper is a part of investigations where the possibility of changing the trajectory of a 3D object approaching a target was verified. During the researches a number of solutions were tested, within which the implementation of a net-gun was also taken into consideration. Therefore the authors of the following study focused on investigations of the impact-contact problem in terms of computational analyses. The paper is an updated and revised version of conference paper [1], and is the next step of the concept presented in the authors' previous papers [2, 3]. The main aim is to present the modelling process and numerical simulations of an impact between two bodies with different geometrical and stiffness characteristics, i.e. the well-known nonlethal net (net-gun) and a small, light flying object [1 - 3]. The solid of revolution was assumed to have much higher stiffness than the net fibre, with a velocity approximately close to the speed of sound, and thus the effectiveness of the net was tested in the most severe working conditions.

The considerations presented can be treated as a sensitivity study of several 1D net configurations (more thoroughly described in Net modelling). A number of cases, including a net with mixed stiffness of its fibres, were analysed and their influence on the 3D rigid object's behaviour was assessed, especially its velocity and trajectory changes. Such factors of the interaction process as time and area of interaction between the simulated bodies was also investigated. Moreover the authors highlighted the importance of a correct contact procedure, which is one of the most essential parameters of such analyses.

The authors came across a paper whose aim was the closest to the area presented [4], where numerical modelling of the interaction between a tennis ball and tennis racket was presented. Also in [5] a comparative study of contact problem solutions were presented, whereas paper [6] covers Finite Element (FE) analyses of several frictionless problems. However, the authors consider the problem of 1D net-gun and 3D body impact interaction presented as a novel one and there are no adequate references or proper literature data which can be used and on which can be based.

Implementation of the contact penalty method to 3D body interaction with 1D net fibre

In the case studied, contact between two bodies: a 3D structural flying object and 1D net fibre elements was adopted and developed based on the segment to segment 3D contact procedure. The theoretical background behind the computational investigations were based on the analytical considerations presented in papers [5, 6]. Analysing the contact problem of the two bodies mentioned, it was assumed that the configuration considered represents a nonlinear problem even when the continuum behaves as a linear elastic material.

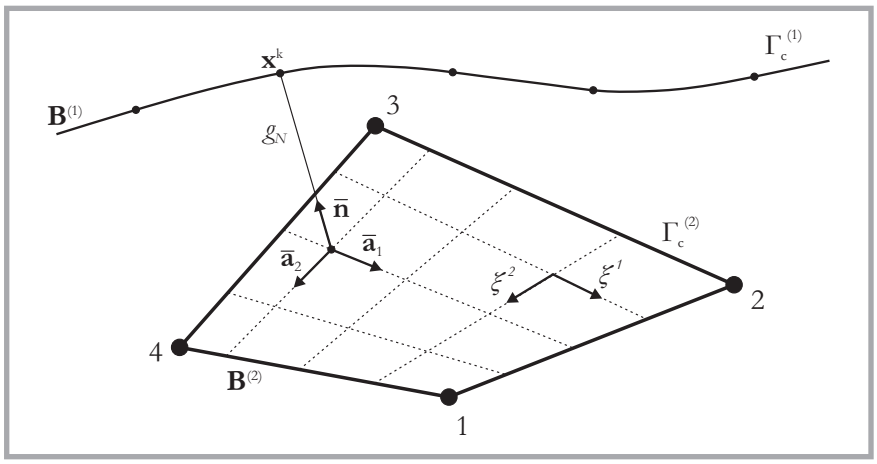

Figure 1. *Geometry of the investigated case [6].*

Theoretical background

In the studies performed two bodies were considered, denoted $B^{(1)}$ (1D fibre net elements) and $B^{(2)}$ (3D flying object) (***Figure 1***).

It was denoted that contact surface $\Gamma_c^{(i)}$ is the part of the body $B^{(1)}$ such that all material points, where contact may occur at any time t, are included. Using a standard notation in contact mechanics slave and master surfaces were assigned to each pair of contact surfaces involved in the problem. In particular, $\Gamma_c^{(i)}$ is taken to be the slave surface and $\Gamma_c^{(2)}$ is the master surface. The condition which must be satisfied is that any slave particle cannot penetrate the master surface. It was assumed that $\bar{\mathbf{x}}$ is the projection point of the current position of slave node $\mathbf{x}^k$ onto the current position of the master surface $\Gamma_c^{(2)}$, defined as follows:

$$\frac{\mathbf{x}^k - \bar{\mathbf{x}}\left(\bar{\xi}^1, \bar{\xi}^2\right)}{\left\|\mathbf{x}^k - \bar{\mathbf{x}}\left(\bar{\xi}^1, \bar{\xi}^2\right)\right\|} \cdot \bar{\mathbf{a}}_\alpha\left(\bar{\xi}^1, \bar{\xi}^2\right) = 0 \quad (1)$$

where: α = 1, 2 and $\bar{\mathbf{a}}_\alpha\left(\bar{\xi}^1, \bar{\xi}^2\right)$ are the tangent covariant base vectors at the point.

The definition of the projection point allows to define the distance between any slave node and the master surface. The normal gap or the penetration g_N for slave node k is defined as the distance between the current position of this node with respect to the master surface $\Gamma_c^{(2)}$:

$$g_N = (\mathbf{x}^k - \bar{\mathbf{x}}) \cdot \bar{\mathbf{n}} \quad (2)$$

where, $\bar{\mathbf{n}}$ refers to the normal to the master face $\Gamma_c^{(2)}$ at point $\bar{\mathbf{x}}$ (***Figure 1***). Normal to be defined using tangent vectors at point $\bar{\mathbf{x}}$. Additionally the following non-penetration conditions were assumed:

$g_N = 0$ full contact;
$g_N > 0$ no contact detected;
$g_N < 0$ penetration between the net fibre and body surface.

In the case analysed, the authors considered the frictional contact and therefore the relative displacement between the contact bodies was also taken into consideration. In such a situation the sliding path of node $\mathbf{x}^k$ over the contact surface $\Gamma_c^{(2)}$ was described by the total tangential relative displacement as follows:

$$g_T = \int_{t_0}^{t} \left\|\dot{\mathbf{g}}_T\right\| dt = \int_{t_0}^{t} \left\|\dot{\bar{\xi}}^\alpha \bar{\mathbf{a}}_\alpha\right\| dt = \int_{t_0}^{t} \sqrt{\dot{\bar{\xi}}^\alpha \dot{\bar{\xi}}^\beta a_{\alpha\beta}}\, dt \quad (3)$$

The time derivatives of parameter $\bar{\xi}^\alpha$ is computed based on relation (1), and for geometrical linear cases can be obtained as follows:

$$a_{\alpha\beta}\dot{\bar{\xi}}^\beta = \left[\dot{\mathbf{x}}^k - \dot{\bar{\mathbf{x}}}\right] \cdot \bar{\mathbf{a}}_\alpha = \dot{g}_{T\alpha} \quad (4)$$

where, $\bar{a}_{\alpha\beta} = \bar{\mathbf{a}}_\beta \cdot \bar{\mathbf{a}}_\alpha$ is the metric tensor at the point $\bar{\mathbf{x}}$ of the master surface $\Gamma_c^{(2)}$.

It was assumed that in the performed analyses between contacting bodies the following constitutive relations according to contact stress tensor $\bar{\mathbf{t}}$ have to be fulfilled:

$$\bar{\mathbf{t}} = \bar{\mathbf{t}}_N + \bar{\mathbf{t}}_T = \bar{t}_N \bar{\mathbf{n}} + \bar{t}_{T\alpha} \bar{\mathbf{a}}^\alpha \quad (5)$$

where: $\bar{t}_N$ is the normal stress, $\bar{t}_T$ is the tangential stress and $\bar{\mathbf{a}}^\alpha$ is the contravariant base vector.

Using the penalty method for normal stress, the constitutive equation is formulated as follows:

$$t = \varepsilon_N g_N \quad (6)$$

where, ε_N is the normal penalty factor.

For the tangential part two modes have to be taken into consideration; stick phase and slip phase. For the first one, a simple linear constitutive model describes the tangential stress as follows:

$$t_{T\alpha}^{stick} = \varepsilon_T g_{T\alpha} \quad (7)$$

where ε_T is the tangential penalty parameter.

During the slip phase the constitutive law describing the tangential stress coming from friction process is defined the following way:

$$t_{T\alpha}^{slip} = -\mu \left|\mathbf{t}_N\right| \frac{\dot{g}_{T\alpha}^{slip}}{\left\|\dot{\mathbf{g}}_{T\alpha}^{slip}\right\|} \quad (8)$$

In the case when the two contacting bodies are considered at time t the principle of virtual work can be written as follows:

$$\sum_{\alpha=1}^{2}\left(\int_{V^{(\alpha)}} \boldsymbol{\sigma}^{(\alpha)} : grad\,\delta\mathbf{u}^{(\alpha)} dV + \right.$$
$$- \int_{V^{(\alpha)}} \rho^{(\alpha)}\left(\mathbf{b}^{(\alpha)} - \ddot{\mathbf{u}}^{(\alpha)}\right)\delta\mathbf{u}^{(\alpha)} dV + \quad (9)$$
$$\left. - \int_{V^{(\alpha)}} \boldsymbol{\sigma}^{(\alpha)} \cdot \mathbf{n} \cdot \delta\mathbf{u}^{(\alpha)} dA \right) - C_c = 0$$

For the penalty formulation the contact contribution C_c is defined as follows:

$$C_c = \int_{Sc} \left(\varepsilon_N g_N \delta g_N + \mathbf{t}_T \cdot \delta g_T\right) dA_k \quad (10)$$

From the finite element formulation the contact contribution (***Equation 10***) for a slave node k is formulated base on the following equation:

$$\begin{aligned} C_c^k &= F_N \delta g_N + \mathbf{F}_T \cdot \delta\mathbf{g}_T = \\ &= t_N A_k \delta g_N + \mathbf{t}_T A_k \delta\mathbf{g}_T = \\ &= t_N A_k \delta g_N + t_{T\alpha} A_k \delta\bar{\xi}^\alpha = \\ &= \delta\mathbf{u}_c^T \mathbf{F}_c = \delta\mathbf{u}_c^T \mathbf{K}_c \Delta\mathbf{u}_c \end{aligned} \quad (11)$$

where, $F_N = t_N A_k$ is the normal force; $F_{T\alpha} = t_{T\alpha} A_k$ is the tangential force; A_k is the area of contact element; $\mathbf{F}_c$ is the contact force vector, $\delta \mathbf{u}_c^T$ is a displacement vector for the contact elements and $\mathbf{K}_c$ is the contact stiffness matrix of contact element containing the tangent stiffness matrix $\mathbf{K}_N$ for the normal contact, the symmetric tangent stiffness matrix $\mathbf{K}_T^{stick}$ for stick condition and the tangent stiffness matrix for the slip case $\mathbf{K}_T^{slip}$ [6]. All above is included in the global nonlinear element equation with penalty approach taken into consideration.

It should be concluded that the most challenging problem in this approach is the contact stiffness assessment, in other words stiffness matrix, which as it will be shown in the next sections of the paper, is dependent on many factors.

Penalty contact implementation in a FE code

The principal feature of the penalty method in explicit FE code is placing normal interface springs between all nodes that penetrate the contact surface [6 - 8]. Currently three different penalty algorithms are available:

1. Standard penalty formulation – typically used in most cases.
2. Segment-based penalty formulation, which is different from a traditional slave node-master segment approach and uses a slave segment – master segment algorithm.
3. Soft constraint penalty formulation, which is implemented in contact between bodies with dissimilar material stiffness. In fact, this approach was used by the authors in the investigations presented.

By using the soft constraint approach, excessive penetration is to be eliminated due to different calculation of the contact stiffness. Therefore, an additional stiffness, apart from the slave and master contact stiffness, is calculated based on the Courant-Friedrichs-Lewy (CFL) stability condition [7] of the local system comprised of two masses of segments connected by a fictional spring. Thus for the parts of different stiffness a stability contact stiffness $k_{cs}(t)$ is determined by [7]:

$$k_{cs}(t) = \frac{1}{2} S_{soft}\, m\left(\frac{1}{\Delta t_{cs}(t)}\right) \qquad (13)$$

where, S_{soft} – scaling factor, m – function dependent on masses of master and slave nodes, Δt_{cs} – initial solution time step (if the solution time step grows, Δt_c is reset to the current time step to prevent unstable behaviour of the simulation).

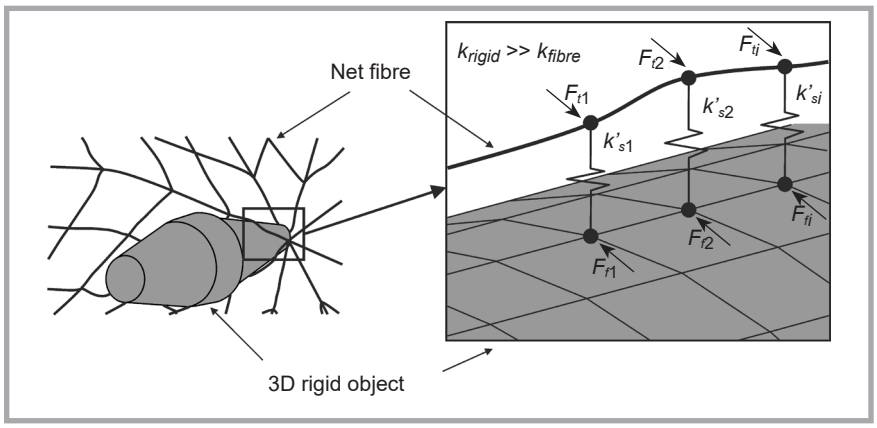

Figure 2. *Force distribution during net – 3D object interaction [3].*

Subsequently the maximum value of the traditionally calculated contact stiffness and the CFL contact stiffness k_{cs} is taken [7]:

$$k_{soft=1} = \max\left\{k_{cs}, k_{soft=0}\right\} \qquad (14)$$

In formula (13) one can see that the contact stiffness depends inter alia on Δt_c, which in turn is estimated based on the following formula:

$$\Delta t = \min\left(\Delta t_{con}, \Delta t_E\right) \qquad (15)$$

where, Δt_{con} – time step size depended on the contact procedure, Δt_{FE} – time step size determined by taking a minimum value over the elements [7]:

$$\Delta t^{n+1} = C \cdot \min\left(\Delta t_1, \Delta t_2, \Delta t_2, ..., \Delta t_N\right) \qquad (16)$$

where, N – number of elements, C – scale factor related to the CFL stability condition; in the investigations presented it was set to 0.67, which together with the proper size of elements guaranteed the stability of computations.

It should be pointed out that in the contact procedure the Coulomb friction model was used which includes the static and kinetic coefficients of friction [7]:

$$\mu = \mu_D + \left(\mu_S - \mu_D\right) e^{-D_C |V_W|} \qquad (18)$$

where, μ_D – dynamic coefficient of friction, μ_S – static coefficient of friction, D_C – exponential coefficient, V_W – relative velocity between two bodies in contact.

Despite the fact that the authors considered friction in the study, it was proved that in such short – lasting interaction it did not have much impact on results obtained, even if its value was changed drastically. Nevertheless for considering the analysis as proper from a physical point of view it was implemented.

Simulated problem

The authors of the paper analysed a contact phenomenon of two parts with different geometrical and stiffness characteristics, i.e. the well-known nonlethal net (net-gun) and 3D flying object. In general, the force distribution within an interaction between the net and 3D object can be illustrated as shown in ***Figure 2***. For the net modelling truss (cable) elements were used, which transfer only axial forces. Therefore during the contact the mesh fibre extends up to breaking. Also different node penetration results in different value of the contact stiffness. Due to the velocities of these two bodies, lateral and friction forces are generated.

From ***Figure 2*** and based on theoretical foundations the following parameters can be distinguished: k_{fibre} – resultant stiffness of the net fibre, k_{object} – resultant stiffness of the solid of revolution, k'_{s1}, ..., k'_{si} – stiffness of the fictional elastic element (dependent on the "contractual" penetration value), F_{f1}, ..., F_{fi} – friction force, F_{T1} , ..., F_{Ti} – tangential force.

Net modelling

The overwhelming net consists of two basic elements. The first is a fibre weave, i.e. the mutual interweaving of lines consequently creating a mesh of netting. The second are segments of a projectile: grapples or piston elements. Their main task is to concentrate the mass required to properly spread the net during flight and to wrap up the possible target. At

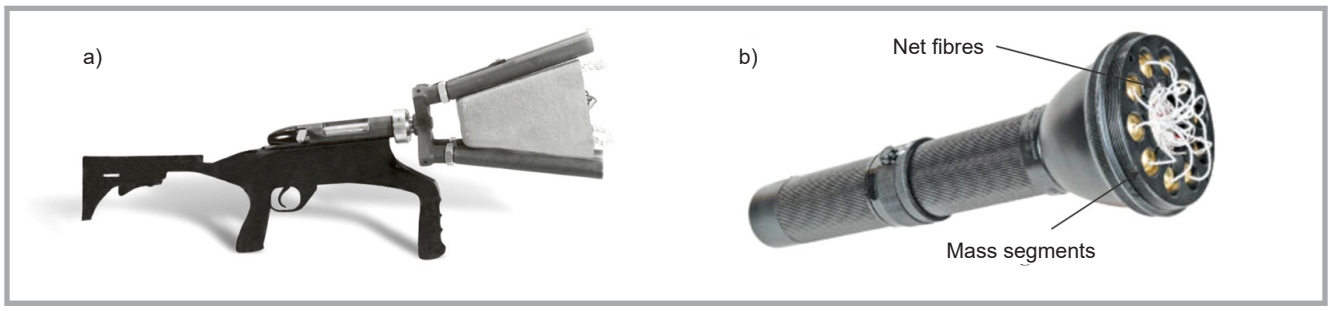

Figure 3. *a) typical net-gun with net launcher [9], b) net inside the gun head [10].*

the initial stage of the shot, the projectile segments have nearly all the kinetic energy from the detonation of gunpowder. In the next stage the net spreads, which is caused by the centrifugal force or angle of segments inside the gun head. An example of such a construction is presented in ***Figure 3***.

In simulations a similar net was taken into consideration, but the process of net modelling started with determination of the geometry and the mesh pattern forming it. This idea came from commonly used and well known solutions, i.e. fishing net and spider web (***Figure 4***).

These two configurations were the basis for a new mesh layout with a geometry similar to a regular octagon with a diameter of 3.1 m and mesh perimeter ratio of 0.265 m. Based on the geometry a numerical model was developed consisting of finite elements [1 - 3], more particular truss (cable) elements with mass elements added to net corners, which simulates weights (piston segments) in the actual net-gun (***Figure 5***). From a physical point of view their purpose is to spread the net after firing.

Based on the previous studies [1 - 3], the authors decided to analyse several net structures with different contact characteristics and geometries with their influence on 3D object behaviour taken into consideration. Thus high-strength aramid fibres (with large stiffness $\mathbf{k_{max}}$) were "mixed" with less stiff material polypropylene (with stiffness $\mathbf{k_{min}}$), which is very often used in sports net manufacturing. The net was mixed only locally, in the area of direct contact with the solid of revolution. Moreover, mass elements were added to the mesh corners similar to passive defence nets used in the protection of military vehicles. Consequently, the following six simulations were carried out (***Figures 6 - 8***, see page 76):

a) with high-strength aramid material:
   - with mass elements added to mesh corners,
   - without mass elements in the mesh corners.
b) with less stiff polypropylene (PP) material:
   - with mass elements added to mesh corners,
   - without mass elements in the mesh corners.
c) with mixed stiffness of fibres (aramid and PP):
   - with mass elements added to mesh corners,
   - without mass elements in the mesh corners.

Due to the fact that in investigations presented it was necessary to simulate contact between the segments of interacting parts as accurately as possible, finer mesh in the area of direct contact was adopted. The FE model of the net consisted of 66768 truss (cable) elements and 63961 nodes. In its corner mass elements were applied, with an overall mass equals to 0.4 kg modelled as 8 mass point elements.

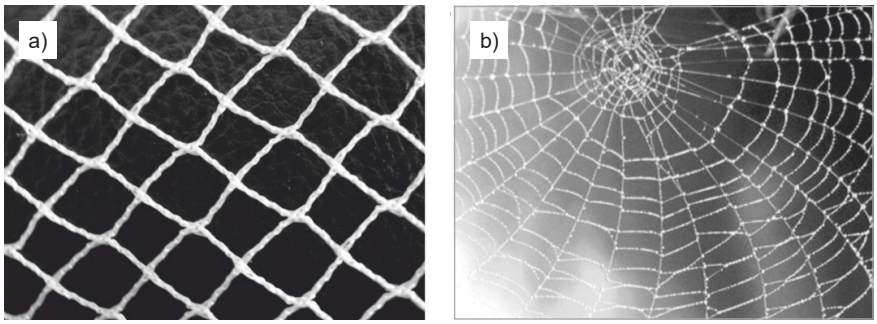

Figure 4. *a) fishing net layout, b) spider web layout [1 - 3]*

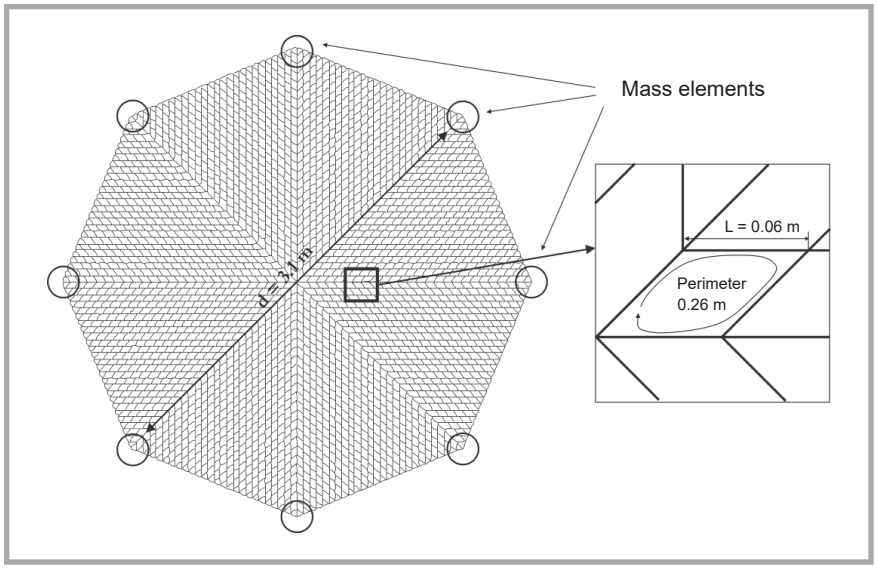

Figure 5. *Octagon-shaped net used in simulations.*

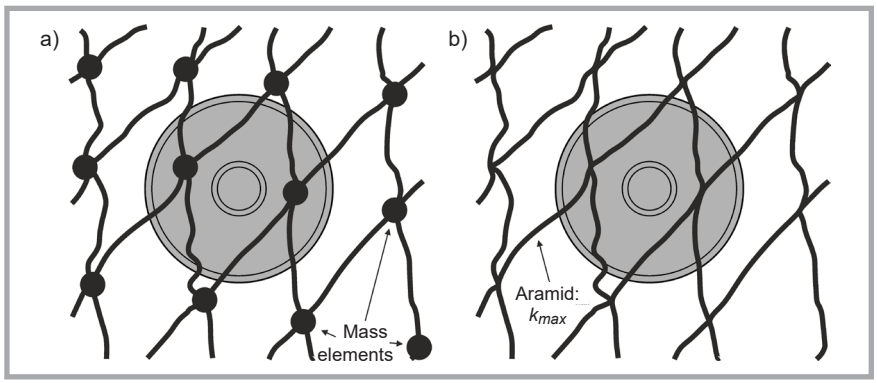

Figure 6. *High-strength aramid net; a) with and b) without mass elements.*

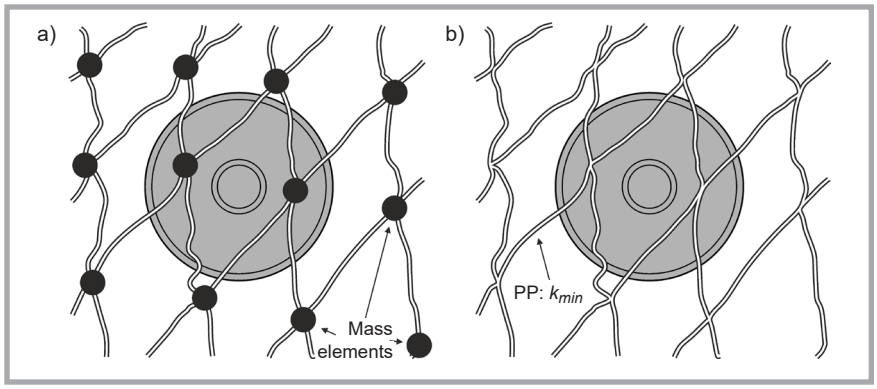

Figure 7. *Polipropylene net; a) with and b) without mass elements.*

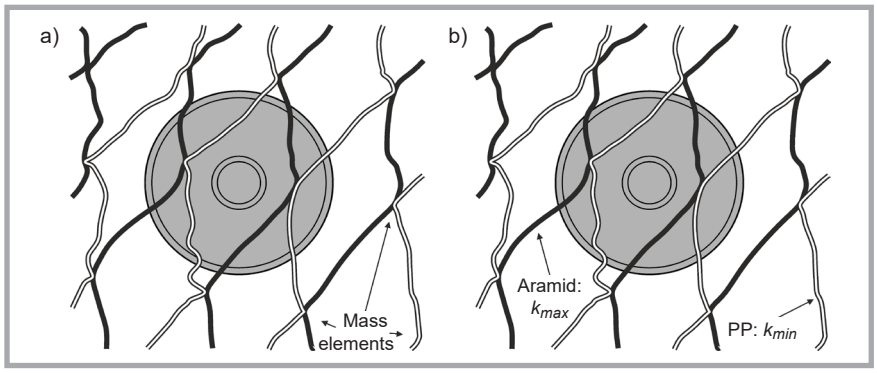

Figure 8. *Aramid - PP net (mixed): a) with and b) without mass elements.*

By adding the mass of the net fibres (1.61 kg: aramid, 1.1 kg: PP, 1.59 kg: mixed) we have the overall mass of the net with piston segments: 2.1 kg, 1.5 kg and 1.99 kg for the aramid, PP and mixed structure respectively. It should be noted that its weight mainly depended on the fibre cross-section (except material), which in this case was approximately 3.14e^{-6} m^2. Both fibres had 1.2 mm thickness (diameter).

Net fibre material characteristics

As mentioned before in studies aramid fibres, more precisely Kevlar 49 was adopted in analyses. Technically speaking, aramid fibres are long-chain synthetic polyamides of high tensile strength, but very low compressive strength. This is why they are widely used in armour and ballistic application, in bicycle tires or as an substitute for asbestos [11]. The name comes from a portmanteau of "aromatic polyamide" [11]. In its fibres the chain molecules are highly oriented along their axis, thus the strength of the chemical bond is easy to exploit.

Kevlar is the registered trademark of the para-aramid synthetic fibre developed at DuPont in 1965 [11, 12]. This material has, among others, high modulus, chemical resistance and toughness, as well as excellent dimensional stability and high cut resistance. Also, its failure energy is relatively high. Its stress-strain characteristic is nearly linear up to breaking: Kevlar 29's tensile elongation at break is ~4%, Kevlar 149's 2%, whereas Kevlar 49's is 3.45% [12], which in fact was used in the investigations presented. Its material parameters of the net fibre described by the stress-strain characteristic obtained from uniaxial tensile experimental tests is presented in ***Figure 9***. Kevlar 49 (stiffness $\mathbf{k_{max}}$) material properties are also listed in ***Table 1***.

In the simulations carried out, material properties of the net were described by the plastic kinematic constitutive model available in the software stated in [7]. Here, the stress-strain curve presented in ***Figure 9*** was replaced by the yield stress value, tangent modulus as well as effective plastic strain for eroding elements, which in fact describes the failure strain criterion for the fibre.

Polypropylene (PP) (also known as polypropene) is a thermoplastic polymer used in a wide variety of applications, such as the automotive industry, packaging, laboratory equipment (resistance to many chemical solvents), etc. Also PP, due to its high fatigue strength, is widely used as material for plastic parts, i.e. living hinges or flip-top bottles. Polypropylene has also been successfully applied in textiles manufacturing, e.g. ropes, thermal underwear and carpets. One such material was implemented in the tests presented, the mechanical properties (stiffness $\mathbf{k_{min}}$) of which are listed in ***Table 2***. To describ PP's material behaviour the piecewise linear plasticity model was adopted [7] with the implementation of the stress-strain characteristic obtained from the quasi-dynamic uniaxial tensile

Table 1. *Aramid material properties with highlighted data implemented in simulations [12].*

Yarn type	Breaking force, N	Tensile strength, MPa	Surface density, g/m^2	Density, kg/m^3	Young's modulus, MPa	Poisson's ratio, -	Elongation at break, -
Multifilament	264	3000	220	**1410**	**1.22E+5**	**0.38**	**3.45**

experimental test carried out, presented in ***Figure 10***.

3D object modelling

Due to the fact that the contact process in the investigations presented played a significant role, a discrete model of the 3D object was modelled using fine and regular mesh which was necessary to simulate the contact procedure between the segments of collaborating parts as accurately and properly as possible. The FE model consisted of 314453 shell elements connected with 368587 nodes. The solid of revolution was assumed to have much higher stiffness than net fibre, with an overall mass of 1.4 kg. Its dimensions were as follows: 0.26 m length and maximum diameter of 0.086 m. The 3D object model implemented is presented in ***Figure 11***.

Simulations characteristics

Initial – boundary conditions

In all cases the movement of the net was simulated through the initial velocity condition applied to all net nodes, with the values: v_{net} = 50 m/s for the translational velocity and ω_{net} = 5.24 rad/s for the rotational. Also for the solid of revolution the same velocities, i.e. translational and rotational were used with the values v_{body} = 300 m/s and ω_{body} = 192 rad/s, correspondingly. Moreover, the same angle of impact was simulated. In all analyses the interaction between bodies was tested using nodes in the surface contact algorithm with the soft constraint option applied, which guaranteed large penetrations not to occur [7]. The parameters were selected and tested through a number of analyses, whose results are not presented in the paper. During analyses the launching process was omitted. A detailed description of such a study can be found in the authors' previous paper [2]. An exemplary 3D object – net system is presented in ***Figure 12*** (see page 78).

Numerical simulations definition

Numerical analyses were performed using an explicit solver with central difference scheme and with the implementation of a modified equation of motion time integration [7]. In this method the acceleration and velocity at t time are given by:

$$\ddot{q}_t = \frac{1}{2\Delta t}\left[q_{t-\Delta t} - 2q_t + q_{t+\Delta t}\right] \quad (19)$$

$$\dot{q}_t = \frac{1}{2\Delta t}\left[q_{t+\Delta t} - q_{t-\Delta t}\right] \quad (20)$$

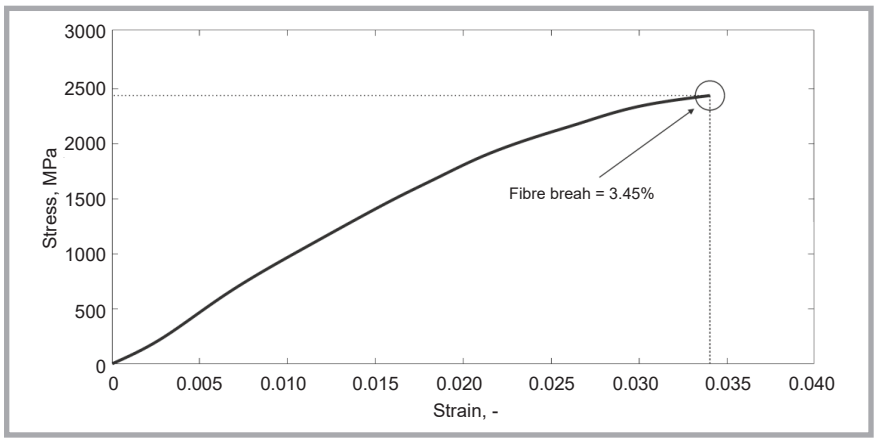

Figure 9. *Kevlar stress-strain characteristic [1 - 3,12].*

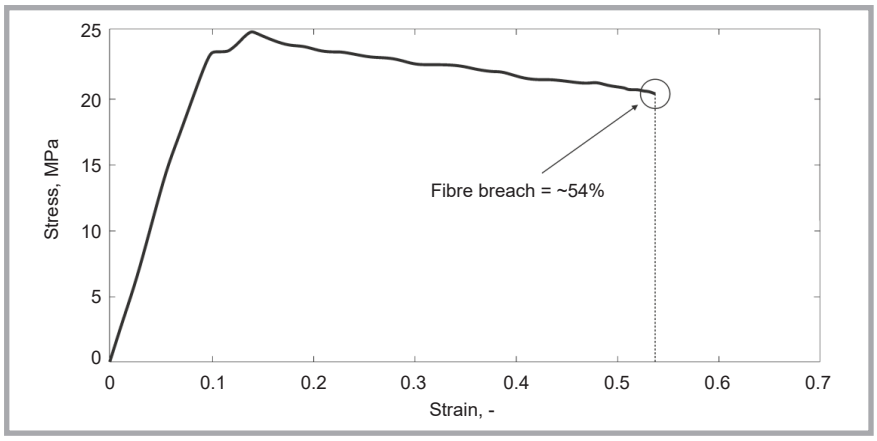

Figure 10. *Polypropylene stress-strain characteristic [3].*

Table 2. *PP material properties with highlighted data implemented in simulations [3].*

Yarn type	Tensile strength, MPa	Density, kg/m^3	Young's modulus, MPa	Poisson's ratio, -	Elongation at break, -
Multifilament	21	**900**	**2.00E+9**	**0.45**	**54**

In the analyses carried out, the stability of computations was guaranteed by the CFL condition [7].

Results and discussion

From the simulations carried out, the general behaviour of the net as well as solid of revolution was obtained. In all analyses due to the contact between the net fibres and object segments the material strain failure criterion was exceeded resulting in fibre breach (material structure continuity loss). The authors presented the velocity, displacement characteristics and resultant force in the chosen element (fibre) of the net. It should be noted, that the displacement (trajectory change) history was taken from the node at the tip of the 3D object. The resultant displace-

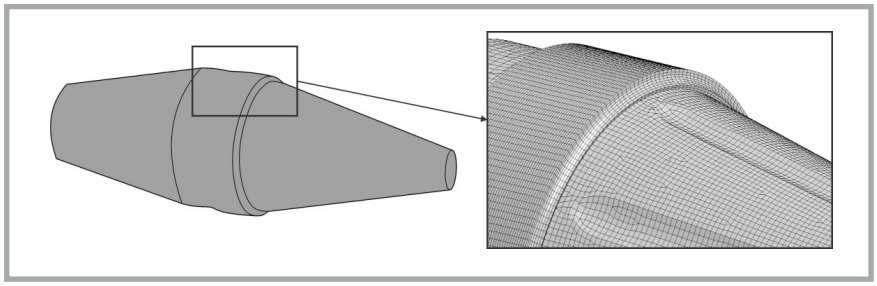

Figure 11. *FE model of the solid of revolution applied in simulations [1 - 3].*

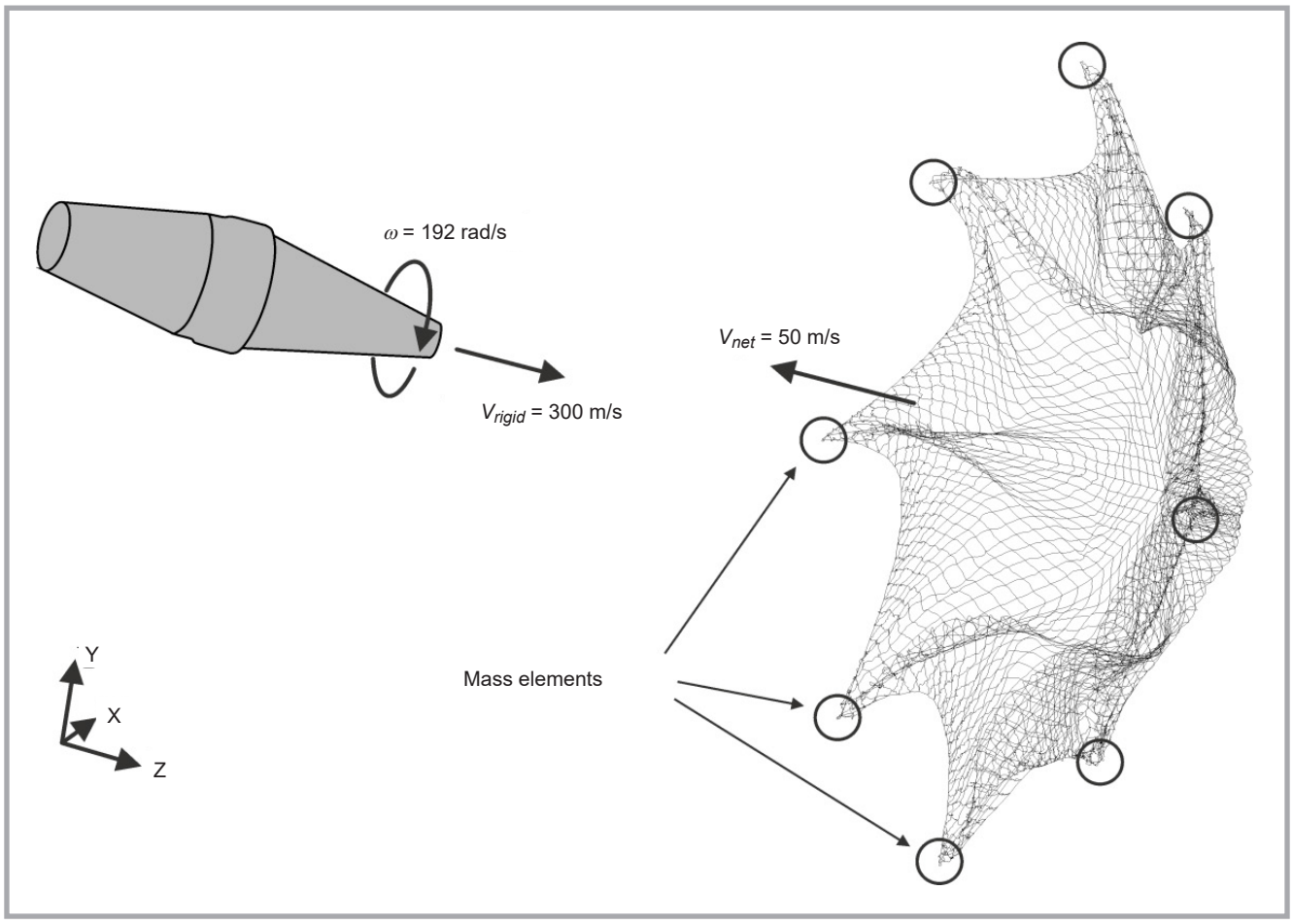

Figure 12. *Initial conditions used in the analysis.*

ment *r* was shown in plane *XY* perpendicular to the flight direction. A schema of the measurement methodology is shown in ***Figure 13***.

In the simulations presented, the fibre net and 3D flying object interaction was obtained. One can see that the 3D object impact influenced the net locally and also globally (***Figure 14***): this phenomenon was noticed in all cases. At the initial stage of interaction the size of the destruction of fibres is a result of the maximum diameter of the 3D object. In the next stages dynamic effects occur and more fibres are damaged. From a numerical point of view the erosion (destruction) of an element takes place when the strain in the element reaches a defined value of the failure criterion, and their stiffness and stress is reset to zero.

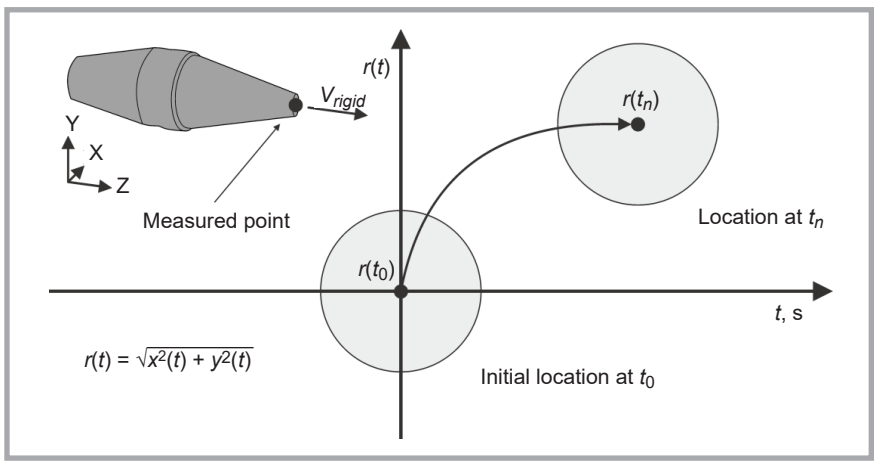

Figure 13. *3D object displacement r(t) measuring schema [3].*

As expected, various contact characteristics in the cases analysed, led to visible changes in the results. From the analysis with a mixed net and polypropylene net, it can be seen that due to the better plasticity and higher elongation at break of PP: 54% (Kevlar: 3.5%), the time of the interaction slightly increased. In order to present this phenomenon, a mixed net without mass elements was chosen, from which the axial force was measured, presented in ***Figure 15*** [3]. The value of the axial force generated in the single finite element with Kevlar properties which was directly in contact reached 7 kN, whereas a smaller axial force was obtained in the truss element of PP: ~94 N [3]

From ***Figures 16*** presenting velocity versus time graphs it can be noticed that in each case the interaction with the net and 3D object led to some differences in velocity decrease during simulation. In the second case it was approximately two times smaller, whereas in the last one (with mixed fibres) it was even three times. Moreover it should be mentioned that the weight of high strength aramid

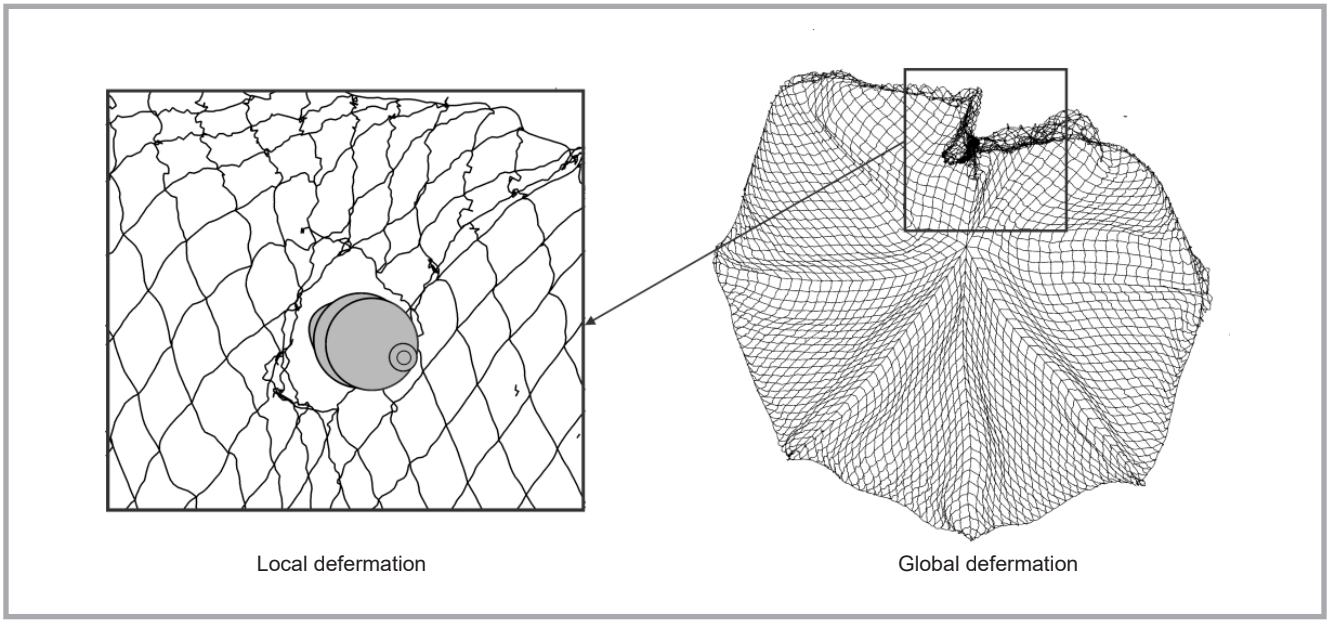

Figure 14. *Local and global influence of 3D object.*

compares more to polypropylene. Therefore the 3D object was not only influenced by the geometrical parameters but also by the physical mass of the net.

The 3D object in the analysis with PP material only had larger velocity after the impact compared to the other cases, despite a slightly longer interaction time. Nevertheless in the case with mixed fibres, the solid of revolution was "longer in contact" with PP parts than high strength aramid nodes. As a consequence, the whole mesh being in contact had a non-symmetric influence on the 3D body's velocity and trajectory change, despite the smaller stiffness and strength of PP (***Figures 16*** & ***17***, see page 80). Also it should be noted that adding mass elements influenced the results even more.

The results presented above are clearly reflected in the resultant displacement (see ***Figure 13***), characteristic of the solid of revolution. It can be seen that not only the velocity drop was larger in the mixed-net case and in all three cases with mass elements. but also the 3D object trajectory changed to a greater extent compared to other cases (***Figure 17***). Nevertheless it can be seen that in the PP case mass elements had a smaller influence on the trajectory change compared to the other two cases.

When we take a closer look at resultant forces of the contact interface (average) of the slave body, i.e. fibres listed in ***Table 3***, we can also see some correlation with the characteristics presented earlier. One can see that different stiffness of the materials together with additional mass elements resulted in a change in the average value of the contact force. It can be noticed that in the mixed-stiffness-net case the values of forces were "between" the other two. Maximum contact forces were obtained in the analyses with aramid net, whereas they were minimum with the net modelled using polypropylene material.

To present a characteristic of the contact procedure more accurately, one case was selected from which data were taken and presented (***Figure 18***, see page 80). In the simulations carried out, node to segment contact was adopted, and therefore slave body (net) nodes were taken into account. Additionally only nodes within meshes closest to the 3D body were selected. The peaks of the force, which are clearly seen on the graph, were caused by discretization of the problem. Maximum values of the force (peaks) are from the ele-

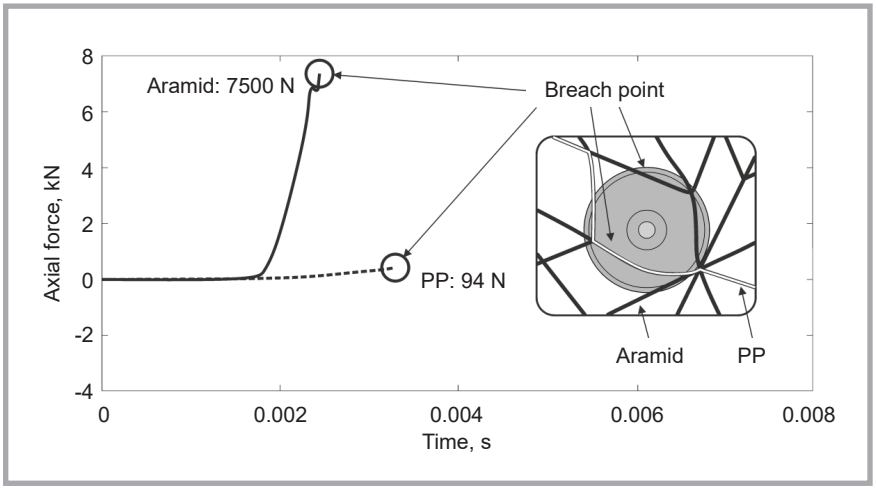

Figure 15. *Force vs. time graph taken from selected elements in contact with the mixed net.*

Table 3. *Average values of resultant contact force in considered cases.*

Aramid net		Polypropylene net		Mixed net	
with mass elements	*without mass elements*	*with mass elements*	*without mass elements*	*with mass elements*	*without mass elements*
586 N	**199 N**	**460 N**	**179 N**	**570 N**	**188 N**

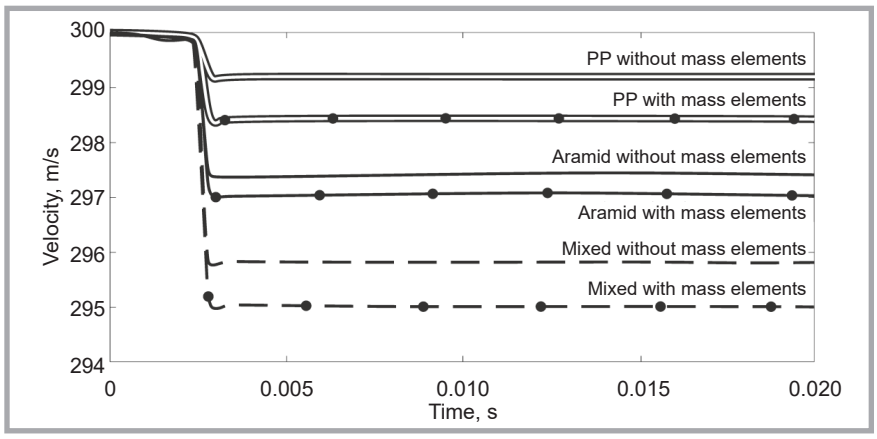

Figure 16. *Comparison graph of resultant velocity in all six cases.*

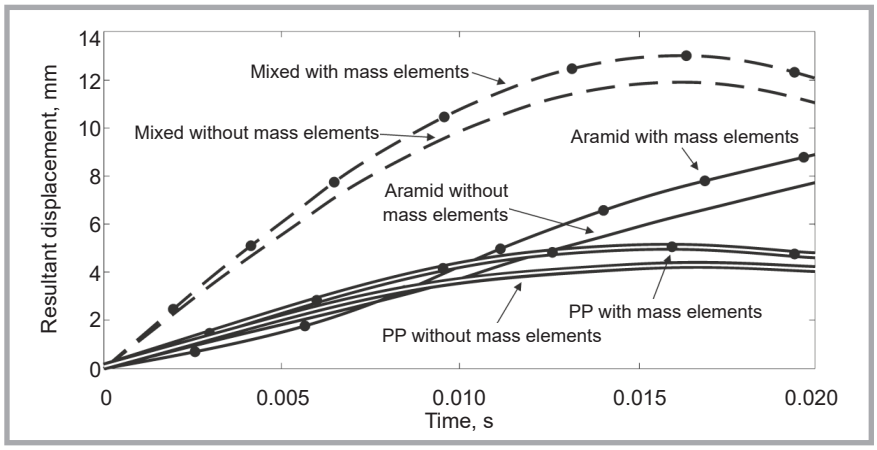

Figure 17. *Comparison graph of resultant displacement r (see **Figure 13**) in all six cases.*

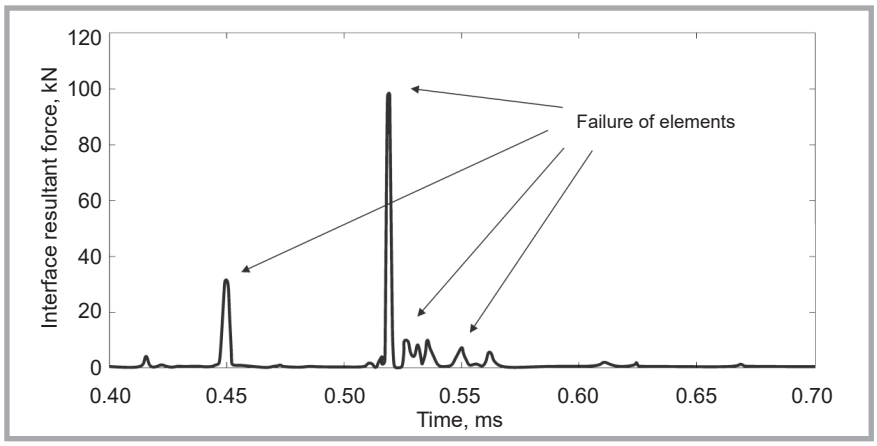

Figure 18. *Resultant contact force vs. time for selected case.*

ments which were directly in contact with the 3D body at the initial stage of interaction. Force peaks are mainly from nodes of the single net mesh in which the 3D object flew (see ***Figure 14***). The force drops when a failure of the fibres (truss elements) occurs. Such large values also resulted from much different stiffness of interacting bodies. Generally it can be explained by the fact that after the erosion of one element, another "stood in the way" of the 3D object, which caused another peak to arise.

Conclusions

This paper is a part of investigations where the possibility of changing the trajectory of an approaching 3D object toward a target was verified. During the researches a number of solutions were tested, within which the implementation of a net-gun was also taken into consideration. The proposition of contact modelling between two bodies with significantly different stiffness and geometry was presented. The main aim of investigations was to assess the possibility of redirecting the flying object due to its contact with the net using numerical methods. As a consequence, a sensitivity study of several 1D net configurations was carried out and their influence on the 3D rigid object' behaviour was assessed, especially its velocity and trajectory changes. Results from simulations proved that the net configurations selected influenced the 3D object in different ways. When analysing the net with added mass elements in corners of the net meshes, the overall larger mass had an impact on 3D behaviour. On the other hand, the time of interaction resulting from the fibre's material properties also gave different results. All in all, the non-symmetric contact characteristic in the case with mixed fibres had a larger impact on the velocity drop and trajectory change of the 3D body. Therefore not only a larger area of interaction, finer mesh and mixed fibres of significantly different stiffness determine the contact effectiveness, as was proved previously [1 - 3], but also the mass, geometry and time of the contact, as is clearly seen in the study presented. Thus the authors assumptions were confirmed. Nevertheless the 3D object could not be stopped by the net, but a redirection of the flight is possible.

The main aim of the numerical analyses carried out was to predict the results of experimental tests and eventually to avoid possible mistakes. The investigations presented allow to draw conclusions and improve the geometry of the high-strength fibre used in actual tests. It should also be highlighted that the assumptions presented were confirmed in field tests and recorded using a high speed digital camera.

The results obtained confirm the applied contact algorithm based on the penalty function working properly. It should be stressed, however, that the effectiveness of the contact was strongly dependent on the mesh quality, value of contact stiffness as well as on the global time step, which, in fact, was scaled by the CFL coefficient and mesh dimensions.

Acknowledgment

The research was carried out under research grant no. O R00 0082 12. This support is gratefully acknowledged.

References

1. Baranowski P, Malachowski J, Niezgoda T. On the Numerical Description of the Contact Problem between a Rigid Flying Object and a Net Structure. In: B.H.V. Topping, P. Iványi, Eds. In: *14th International Conference on Civil, Structural and Environmental Engineering Computing*. Civil-Comp Press, Stirlingshire, UK, Paper 57; doi:10.4203/ccp.102.57, 2013.
2. Baranowski P, Bukała J, Damaziak K, Małachowski J, Mazurkiewicz Ł, Niezgoda T. Numerical Tests of Impact Process Between Net Structure and Rigid Object During Flight. (in Polish). *Problems of Mechatronics. Armament, Aviation, Safety Engineering* 2013; 4, 1(11): 63-80.
3. Baranowski P, Małachowski J, Niezgoda T, Mazurkiewicz L, Damaziak K. Dynamic contact modelling between two bodies with significantly different stiffness. CMM-2013 20th International Conference on Computer Methods in Mechanics, Poznań, August 27-31, 2013; In: Łodygowski T, Rakowski J, Litewka P. Eds. *Recent Advances in Computational Mechanics* 2014: 165-172.
4. Abaqus. Tennis racket simulation using Abaqus. Introduction to Abaqus, Copyright Dassault Systems, 2007.
5. Wriggers P, Van TV, Stein E. Finite element formulation of large deformation impact-contact problems with friction. *Computers and Structures* 1990; 37: 319-333.
6. Vulovic S, Zivkovic M, Grujovic N, Slavkovic RA. Comparative study of contact problems solution based on the penalty and Lagrange multiplier approaches. *J. Serbian Society for Computational Mechanics* 2007; 1(1): 174-183.
7. Hallquist JO. *LS-Dyna: Theoretical manual*. Ed. California Livermore Software Technology Corporation, 2003.
8. Bajer C. Numerical modelling of space-time dynamic contact problems (in Polish). Ed. IPPT PAN, Warsaw, 1997.
9. http://www.codaenterprises.com/products.html
10. http://www.lawenforcementmall.com/talon.php
11. Fejdyś M, Łandwijt M. Technical fibres enhancing composite materials (in Polish). *Technical Textiles* 2010; 1-2: 12-22.
12. Kevlar aramid fiber technical guide, DuPont Advanced Fiber Systems, H-77848 4/00 USA.

Received 24.03.2015 Reviewed 30.04.2015

Conference and Seminar - Modern Textile and Fashion Industry (Including Design)

were held on 14 and 15 September 2015 at the Expo Hall, Łódź, Poland

The following lecturers and discussions were held:

CONFERENCE

Marek Gajewski – Representative of the Marshal Office of Łódź Voivodeship, Poland	Opening of the conference. Development strategy of the Łódź Region.
Prof. Zofia Wysokińska, Ph.D., D.Sc. - University of Lodz, Poland	Trends and tendencies of the modern textile industry: Poland, Europe, World, and the position of the textile industry of the Łódź Region.
Assoc. prof. Dana Křemenáková, Ph.D., D.Sc., Eng.- Technical University of Liberec, Czech Republic; and Libuše Fouňová, Eng. - CLUTEX	Clutex - Clusters of Technical Textiles as an instrument of the the development of the textile and clothing industries.
Prof. Józef Masajtis, Ph.D., D.Sc., Eng. - Lodz University of Technology, Poland	Design - a chance for the development of SMEs, cities and regions.
Katarzyna Kędzia, M.Sc. - Lodz University of Technology, Poland; The One Design Company, Zgierz, Poland	Designing for corporations.
Dionizy Smoleń - PwC Ltd., Lodz, Poland	Creating sectoral policies for the Łódź Region.
Prof. Marek Snycerski, Ph.D., D.Sc., Eng. - Lodz University of Technology, Poland	Textile innovations. The possibility for Łódź industry.
Prof. Izabella Krucińska, Ph.D., D.Sc., Eng. - Lodz University of Technology, Poland	Center of Creative Technologies – 'Innovative Textiles 2020+'.
Marzanna Lesiakowska-Jabłońska, Ph.D., Eng. - Viamoda, Warsaw, Poland	The innovative potential of the textile industry.
Michał Juda – showroom.pl	'SHWRM' as an example of a multibrand portal of gathering the creators of Polish fashion.
Aleksandra Wereszka, Ph.D. - Lodz University of Technology, Poland	New concepts in underwear design and technology.
Arkadiusz Taraska – fashion designer	Apparel designing, building of the brand.
Klara Tolnai – Tok Company, Konstantynów Łódzki, Poland	Presentation of a company from the Łódź Region.
Magdalena Buczak – Slow Group, Warsaw, Poland	Slow fashion - a new trend in the fashion.

SEMINAR

Prof. Józef Masajtis, Ph.D., D.Sc., Eng. - Lodz University of Technology, Poland	Designing engineers and designers for the modern textile and fashion industries.
Prof. Zbigniew Mikołajczyk, Ph.D., D.Sc., Eng. - Lodz University of Technology, Poland	Modern technologies for knitting.
Zbigniew Kucharski, Ph. D. - MARTELLO Ltd., Lodz, Poland	Presentation - case study.
Bogdan Sitarz, M.Sc., Eng. - Bowi-Styl, Lodz, Poland	Presentation - case study.
Prof. Marek Snycerski, Ph.D., D.Sc., Eng. - Lodz University of Technology, Poland	Modern technologies for weaving.
Maria Dąbrowska, M.Sc., Eng. - OPTEX Co., Opoczno, Poland	Presentation - case study.
Jacek Godzisz, M.Sc., Eng. – Andropol Ltd., Andrychów, Poland	Presentation - case study.
Prof. Monika Kostrzewa, Ph.D., D.Sc. – Adam Mickiewicz University in Poznań, Faculty of Pedagogy and Fine Arts in Kalisz, Poland	'Design thinking' - in the modern textile industry.
Prof. Elżbieta Kędzia - Lodz University of Technology, Poland	Presentation - case study.
Magdalena Owczarek, Ph.D., Eng. - Lodz University of Technology, Poland	Presentation - case study.
Maciej Boguń, Ph.D., D.Sc. - Lodz University of Technology, Poland	Textiles for healthcare.
Joanna Matras, M.Sc., Eng. – TRICOMED Co., Lodz, Poland	Presentation - case study.
Witold Sujka, Ph.D., Eng. – TRICOMED Co., Lodz, Poland	Presentation - case study.

About 300 participants including 150 entrepreneurs took part in these events.

For more information please contact: www.rsi.lodzkie.pl